Efficacy and improved resistance potential of a cofactor-independent InhA inhibitor of *Mycobacterium tuberculosis* in a C3HeB/FeJ mouse model

Running title: Efficacy of AN12855 in C3HeB/FeJ mice

Authors:

Gregory T. Robertson[1]*, Victoria A. Ektnitphong[1], Michael S. Scherman[1], Matthew B. McNeil[2], Devon Dennison[2], Aaron Korkegian[2], Anthony J. Smith[1], Jason Halladay[3], David S. Carter[3], Yi Xia[3], Yasheen Zhou[3], Wai Choi[3], Pam Berry[3], Weimin Mao[3], Vincent Hernandez[3], M. R. K. Alley[3], Tanya Parish[2], Anne J. Lenaerts[1]

Affiliations:

[1]Mycobacteria Research Laboratories, Department of Microbiology, Immunology and Pathology, Colorado State University, Fort Collins, CO 80523 USA.

[2]TB Discovery Research, Infectious Disease Research Institute, 1616 Eastlake Ave E, Suite 400, Seattle, WA, 98102, USA.

[3]Anacor Pharmaceuticals, 1020 E Meadow Cir, Palo Alto, CA 94303, USA

*To whom correspondence should be addressed:

gregory.robertson@colostate.edu

tel +1 970-971-4117

Abstract:

AN12855 is a direct, cofactor-independent inhibitor of InhA in *Mycobacterium tuberculosis*. In the C3HeB/FeJ mouse model with caseous necrotic lung lesions, AN12855 proved efficacious with a significantly lower resistance frequency compared to isoniazid. AN12855 drug levels were better retained in necrotic lesions and caseum where the majority of hard to treat, extracellular bacilli reside. Owing to these combined attributes, AN12855 represents a promising alternative to the frontline anti-tuberculosis agent isoniazid.

Keywords: caseum, necrotic lesions, tuberculosis, C3HeB/FeJ mice, isoniazid, drug development, antimicrobial resistance

A previous study described the identification of a novel diazaborine scaffold that inhibits enoyl-ACP reductase (InhA), a clinically-proven drug target in *Mycobacterium tuberculosis* (1). The lead compound, ethylsulfonyl benzodiazaborine (AN12855; Fig. 2C), binds to and inhibits InhA with sub-micromolar affinity through a novel cofactor-independent mechanism (1). Unlike isoniazid (INH; Fig. 2C), which requires prodrug activation by the peroxidase-catalase enzyme, KatG (2), AN12855 binds directly to InhA, occupying both the cofactor and substrate-binding sites (1). These features impart two direct benefits to the inhibitor: (i) potent activity against common isoniazid-resistant strains with mutations affecting the non-essential KatG activation enzyme (3) and (ii) improved resistance frequency compared to INH, reflecting a unique binding pocket and essentiality of the InhA target (1). Thus, AN12855 retains potent activity against both drug-susceptible and drug-resistant strains of *M. tuberculosis* including those with *katG* and *inhA* coding sequence mutations (1). AN12855 is not cytotoxic against HepG2 or THP-1 cell lines, shows no tolerability issues in mice at doses up to 200 mg/kg, and exhibits *in vivo* efficacy following oral delivery in murine acute and chronic tuberculosis (TB) efficacy models (1). Given the proven clinical utility of the target, its unique co-factor independent mode-of-action, and retained activity against clinically relevant *katG* and *inhA* INH-resistant mutants, the diazoborine AN12855 is viewed as a novel compound with utility as both a possible replacement for INH in the standard frontline regimen but also for inclusion in combination with newer regimens under development. Owing to its established mode-of-action, it is anticipated that this will translate into faster killing early, and by having this early killing activity, could lead to treatment shortening when used in combination with other drugs. Thus, AN12855 was reported to represent a promising lead compound for the development of novel TB therapeutics.

A hallmark of active *M. tuberculosis* infection in humans is the development of pulmonary granulomas with central caseous necrosis (4-8). Unlike conventional TB mouse efficacy models, where granulomas in lungs are exclusively cellular, the C3HeB/FeJ mouse model develops well-defined, necrotic lesions with caseous centers that resemble more closely human lesions upon a *M. tuberculosis* infection (4, 9-11). To begin to understand the impact of advanced lung pathology on treatment outcome, we employed this mouse model to evaluate efficacy, resistance development, and tissue distribution more comprehensively for these distinct InhA inhibitors *in vivo*. In an initial study, we compared the efficacy in lungs of C3HeB/FeJ mice following 2, 4 and 8 weeks of treatment with INH or AN12855. In addition, the emergence of drug-resistance was studied during therapy. Thereto, female C3HeB/FeJ mice were infected by low dose aerosol with *M. tuberculosis* Erdman, as described (12, 13). Lung burdens increased from a mean CFU count of 2.09 (SEM 1.54) $\log_{10}$ one day following infection, to an average of 7.61 (SEM 0.18) $\log_{10}$ at the start of treatment on day 68 (Fig. 1). Gross pathology analysis revealed heterogeneous cellular and caseous necrotic lesions in lungs of individual mice (11), indicating the desired pulmonary pathology had fully developed prior to the start of treatment (data not shown). Groups of eight mice each were treated as described ((1) and Fig. 1). INH given at 25 mg/kg in sterile water reduced lung burdens from the start of treatment by 0.71 logs at 2 weeks and by 0.94 and 0.98 logs at weeks 4 and 8, respectively (Table 1 and Fig. 1). These differences were not statistically significant ($P > 0.05$). AN12855 given at 100 mg/kg in 1% [w/v] methyl cellulose, 0.1% [v:v] polysorbate-80 showed greater bactericidal activity by promoting significant reductions in lung burdens from the start of treatment of 1.25 logs at 2 weeks ($P < 0.001$) and 1.48 ($P = 0.001$) and 1.34 logs ($P < 0.05$) at weeks 4 and 8, respectively (Table 1 and Fig. 1). The better overall activity of AN12855 in this model was reproducible in a second independent C3HeB/FeJ study (not shown). The improved

activity of AN12855 over INH in C3HeB/FeJ mice, is in contrast to the earlier reported results in the acute GKO mouse model or in chronically infected BALB/c mice, where similar efficacy was achieved for INH and AN12855 (1). Thus, in the results presented here, AN12855 showed superior efficacy when compared to INH at the prescribed doses in the C3HeB/FeJ mouse model with advanced lung pathology.

Due to the high bacterial numbers in the C3HeB/FeJ mouse model, it is an ideal model and useful tool for studying resistance frequencies *in vivo*. Earlier published studies have shown a greater propensity for expansion of drug resistance in C3HeB/FeJ mice compared to *M. tuberculosis*-infected BALB/c mice (4). We therefore considered the hypothesis that emergence of appreciable drug-resistance to INH contributes to the difference in efficacy observed in C3HeB/FeJ mice between both compounds. To test this hypothesis, lung homogenates from each time point were co-plated on 7H11-OADC agar medium with AN12855 at 1.25 mg/L or INH at 0.625 mg/L, representing the lowest selective drug concentrations to give rise to genetically-stable drug-resistant isolates using high-titer *M. tuberculosis* Erdman cultures *in vitro* (1). Consistent with previous studies (4), spontaneous INH-resistance was detected under these conditions at a frequency of 7×10^{-6} (i.e., 0.001% INH-resistant, as defined above) prior to the initiation of treatment in the lungs of six of eight *M. tuberculosis* Erdman infected C3HeB/FeJ mice (Table 1). INH resistance arose at a frequency of 1×10^{-6} under the same selection conditions *in vitro*. In contrast, the frequency of AN12855 resistant mutants recovered from *M. tuberculosis* Erdman infected C3HeB/FeJ mice prior to the start of treatment was below the limit of detection $< 3\times10^{-7}$ (<0.0006% AN12855-resistant; as defined above). AN12855 resistance arose at a frequency of 4×10^{-7} under identical selection conditions *in vitro*. Similar *in vivo* spontaneous resistance

105 frequencies were observed in a second independent C3HeB/FeJ infection study, indicating the
106 results were reproducible (not shown).

107 Initiation of drug treatment with INH in monotherapy resulted in an increase in the
108 proportion of INH-resistant to -susceptible subpopulations such that all of the mice in the INH
109 treatment group had discernable drug-resistant bacilli by the end of treatment (Table 1). The
110 proportion of INH-resistant bacteria within this treatment group increased from 0.001% prior to
111 the initiation of treatment to 29% by the end of treatment (Table 1). As expected, resistance to INH
112 was associated with a spectrum of single nucleotide polymorphisms in the nonessential *katG* gene
113 (i.e., 323A>C, 514G>A (isolated twice), 566A>T, 982T>C, 1431G>A, 1712G>A) promoting
114 changes in the KatG amino acid sequence (i.e., H108P, A172T (isolated twice), D189V, W328R,
115 W477X, R571H). This diversity of recovered *katG* alleles, indicates that *in vivo* INH-resistance
116 did not arise from one single dominant resistant clone. In contrast, resistance to AN12855 was
117 observed in only one of eight mice, and at the 8-week time point only (Table 1). Although the
118 overall proportion of resistance for AN12855 was much lower than that observed for INH
119 (compare 29% INH-resistance compared to 0.037% AN12855-resistance at the end of treatment),
120 the number of AN12855-resistant bacilli observed in this single mouse was high relative to the
121 total bacterial burden (see Table 1). Sequence analysis of five single colony isolates from this
122 mouse revealed a common 287G>T mutation in *inhA* resulting in $InhA_{G96V}$. Given that a wider
123 spectrum of AN12855-resistant clones have been obtained *in vitro* (i.e., G96A (isolated twice),
124 IG96V, I16T, D148G, P151S, R195Q, I202T, E219A and also a C-15-T mutation in the *fabGI-*
125 *inhA* promoter (isolated twice) (this work and (1))), it seems likely that the resistance observed in
126 this mouse was the result of expansion of a single AN12855-resistant clone.

Evaluation of an AN12855-resistant clone bearing $InhA_{G96V}$ by broth microdilution MIC (14), revealed a > 122-fold shift in MIC to AN12855, but no appreciable shift in MIC for INH (Table 2). In contrast, *in vitro* isolated *M. tuberculosis* Erdman bearing a *fabG1-inhA* C-15-T promoter mutation, which increases cellular abundance of InhA (3, 15), conferred cross-resistance to both INH and AN12855, as expected (Table 2; (1)). All MIC values were reproducible in two or more independent studies, and no appreciable MIC shifts were observed for rifampicin (≤ 2-fold). Given the proximity of G96 to the sulphonyl group of AN12855 in the InhA-AN12855 co-crystal (1), we predict that the G96V substitution interferes with docking of AN12855. This is supported by the observation that elevated MICs for AN12855 were also observed for an *in vitro* isolated AN12855-resistant strain bearing the less bulky $InhA_{G96A}$ substitution (Table 2). Additional studies are required to validate this experimentally. Taken together, these data indicate that AN12855 remains on target *in vivo* and that direct InhA inhibitors as a class of compounds, could potentially have reduced potency against the 20% of clinical INH resistant strains that have mutations in the *fabG1-inhA* promoter (3, 15). These findings should be taken into account when determining doses needed for strain coverage in TB patients.

The expansion of diverse INH-resistant subpopulations was, in part, responsible for the more limited efficacy of INH versus the AN12855 group as roughly 29% of the total bacterial population was INH-resistant by the end of treatment. However, it seems unlikely to be the only contributing factor as differences in efficacy were observed after only 2 weeks of treatment in C3HeB/FeJ mice, which is prior to the significant expansion of INH-resistance (see Fig. 1). This prompted us to investigate the systemic and local drug exposure of both drugs by determining the pharmacokinetic (PK) and tissue distribution properties (16) in the C3HeB/FeJ mouse model. For this purpose, mice were divided into treatment groups ten weeks after aerosol infection, and

150 therapy administered as above for seven consecutive days. Plasma, regions of uninvolved lung,
151 whole necrotic Type I lesions, and caseum from the core of Type I lesions (11), were dissected
152 from individual C3HeB/FeJ mice, as described in (9). Samples were collected at 0.5hrs, 6 hrs and
153 24 hrs for INH and 2 hrs, 6 hrs, and 24 hrs for AN12855 based on T_{max} values from previously
154 published plasma PK studies (1, 17). Results showed that 2 hrs after dosing, AN12855 drug levels
155 were highest in plasma and uninvolved lung and lowest in necrotic lesions and caseum (Fig. 2D,
156 top panel, filled triangles and Fig. 2E). Drug levels in all lung compartments were much higher
157 overall for AN12855 than for INH, partly reflecting differences in administered drug doses, but
158 also suggesting better drug distribution into tissues/lesions in general (Fig. 2E). As expected, both
159 AN12855 and INH were rapidly cleared from plasma over time (Fig. 2D and 2E; (1, 17)). INH
160 was readily cleared from uninvolved lung, necrotic lesions and caseum also, with drug levels
161 falling below the limits of quantification by 24 hours (Fig. 2E). Contrary to the INH tissue
162 distribution data, AN12855 was found to partition into lung, necrotic lesions and caseum early,
163 and to a remarkable greater extent (Fig. 2D and 2E). In addition, AN12855, showed selective
164 retention in lung lesions compared to plasma, especially in necrotic lesions and caseum (Fig. 2D
165 and 2E), at levels approaching or exceeding the plasma protein bound MIC (i.e., 0.5 mg/L; (1)).
166 The data supports the hypothesis that the physiochemical properties of AN12855 promote better
167 lesion distribution and retention relative to INH in an animal model presenting with advanced
168 necrotic lung disease. As the majority of extracellular bacilli reside in the caseous necrotic lesion
169 cores of C3HeB/FeJ mice (4), the improved drug exposure inside pulmonary lesions is likely to
170 contribute to the increased efficacy of AN12855 over INH in this TB mouse efficacy model. Other
171 explanations, such as reduced activation of the INH prodrug in hypoxic, necrotic lesions (4, 9-11),

seem less likely given that the active INH-NAD+ adduct is readily detected in the Wayne's anaerobic dormancy model *in vitro* (18).

Our data also suggest a possible advantage of the diazoborine AN12855 with regard to lower resistance development *in vivo*. Although encouraging, placing these resistance data into clinical context will require evaluation of wild-type MIC distributions to determine a clinically meaningful susceptibility breakpoint for AN12855 in future studies. We note also that the *in vivo* emergence of INH resistance observed herein in C3HeB/FeJ mice, more closely resembles that observed in *in vitro* time-kill assays or in the hollow-fiber model (1, 19). These data are in contrast to a complete lack of INH resistance emergence in *M. tuberculosis*-infected guinea pigs (20). As INH-resistant isolates are readily detected in sputum of TB infected patients, these findings suggest that the C3HeB/FeJ TB mouse efficacy model might better reflect the human situation in terms of resistance frequency and therefore could be a good tool for studying resistance of single drugs and potentially drug combinations for which other models can rarely provide data. Collectively, these combined data support a model that better drug distribution/retention of the diazaborine AN12855 in necrotic lesions and lower resistance potential make this a better compound for a disease state modeled in C3HeB/FeJ mice and seen in human TB patients.

Author Contribution

GTR, AJL, MBM, TP, and MRKA designed the experiments; VAE, MSS, MBM, DD, AK, AJS, JH, DSC, YX, YZ, WC, PB, WM, VH performed the experiments; GTR, MBM, TP, AJL and MRKA analyzed data; GTR, MBM, TP, MRKA and AJL wrote the paper.

Conflict of interest

The authors declare no conflict of interest.

Funding

This research was supported with funding from the Bill and Melinda Gates Foundation through a subcontract from Anacor Pharmaceuticals to Colorado State University.

Antimicrobial Agents and Chemotherapy

References

1. Xia Y, Zhou Y, Carter DS, McNeil MB, Choi W, Halladay J, Berry PW, Mao W, Hernandez V, O'Malley T, Korkegian A, Sunde B, Flint L, Woolhiser LK, Scherman MS, Gruppo V, Hastings C, Robertson GT, Ioerger TR, Sacchettini J, Tonge PJ, Lenaerts AJ, Parish T, Alley M. 2018. Discovery of a cofactor-independent inhibitor of *Mycobacterium tuberculosis* InhA. Life Science Alliance 1.
2. Zhao X, Yu H, Yu S, Wang F, Sacchettini JC, Magliozzo RS. 2006. Hydrogen peroxide-mediated isoniazid activation catalyzed by *Mycobacterium tuberculosis* catalase-peroxidase (KatG) and its S315T mutant. Biochemistry 45:4131-40.
3. Seifert M, Catanzaro D, Catanzaro A, Rodwell TC. 2015. Genetic mutations associated with isoniazid resistance in *Mycobacterium tuberculosis*: a systematic review. PLoS One 10:e0119628.
4. Driver ER, Ryan GJ, Hoff DR, Irwin SM, Basaraba RJ, Kramnik I, Lenaerts AJ. 2012. Evaluation of a mouse model of necrotic granuloma formation using C3HeB/FeJ mice for testing of drugs against *Mycobacterium tuberculosis*. Antimicrob Agents Chemother 56:3181-95.
5. Harper J, Skerry C, Davis SL, Tasneen R, Weir M, Kramnik I, Bishai WR, Pomper MG, Nuermberger EL, Jain SK. 2012. Mouse model of necrotic tuberculosis granulomas develops hypoxic lesions. J Infect Dis 205:595-602.
6. Pichugin AV, Yan BS, Sloutsky A, Kobzik L, Kramnik I. 2009. Dominant role of the *sst1* locus in pathogenesis of necrotizing lung granulomas during chronic tuberculosis infection and reactivation in genetically resistant hosts. Am J Pathol 174:2190-201.
7. Dutta NK, Illei PB, Jain SK, Karakousis PC. 2014. Characterization of a novel necrotic granuloma model of latent tuberculosis infection and reactivation in mice. Am J Pathol 184:2045-55.
8. Ordonez AA, Tasneen R, Pokkali S, Xu Z, Converse PJ, Klunk MH, Mollura DJ, Nuermberger EL, Jain SK. 2016. Mouse model of pulmonary cavitary tuberculosis and expression of matrix metalloproteinase-9. Dis Model Mech 9:779-88.
9. Irwin SM, Prideaux B, Lyon ER, Zimmerman MD, Brooks EJ, Schrupp CA, Chen C, Reichlen MJ, Asay BC, Voskuil MI, Nuermberger EL, Andries K, Lyons MA, Dartois V, Lenaerts AJ. 2016. Bedaquiline and Pyrazinamide Treatment Responses Are Affected by Pulmonary Lesion Heterogeneity in *Mycobacterium tuberculosis* Infected C3HeB/FeJ Mice. ACS Infect Dis 2:251-267.
10. Lanoix JP, Lenaerts AJ, Nuermberger EL. 2015. Heterogeneous disease progression and treatment response in a C3HeB/FeJ mouse model of tuberculosis. Dis Model Mech 8:603-10.
11. Irwin SM, Driver E, Lyon E, Schrupp C, Ryan G, Gonzalez-Juarrero M, Basaraba RJ, Nuermberger EL, Lenaerts AJ. 2015. Presence of multiple lesion types with vastly different microenvironments in C3HeB/FeJ mice following aerosol infection with *Mycobacterium tuberculosis*. Dis Model Mech 8:591-602.
12. Kelly BP, Furney SK, Jessen MT, Orme IM. 1996. Low-dose aerosol infection model for testing drugs for efficacy against *Mycobacterium tuberculosis*. Antimicrob Agents Chemother 40:2809-12.
13. Lenaerts AJ, Gruppo V, Marietta KS, Johnson CM, Driscoll DK, Tompkins NM, Rose JD, Reynolds RC, Orme IM. 2005. Preclinical testing of the nitroimidazopyran PA-824 for

activity against *Mycobacterium tuberculosis* in a series of in vitro and in vivo models. Antimicrob Agents Chemother 49:2294-301.

14. Ollinger J, Bailey MA, Moraski GC, Casey A, Florio S, Alling T, Miller MJ, Parish T. 2013. A dual read-out assay to evaluate the potency of compounds active against *Mycobacterium tuberculosis*. PLoS One 8:e60531.
15. Vilcheze C, Wang F, Arai M, Hazbon MH, Colangeli R, Kremer L, Weisbrod TR, Alland D, Sacchettini JC, Jacobs WR, Jr. 2006. Transfer of a point mutation in *Mycobacterium tuberculosis inhA* resolves the target of isoniazid. Nat Med 12:1027-9.
16. Prideaux B, Via LE, Zimmerman MD, Eum S, Sarathy J, O'Brien P, Chen C, Kaya F, Weiner DM, Chen PY, Song T, Lee M, Shim TS, Cho JS, Kim W, Cho SN, Olivier KN, Barry CE, 3rd, Dartois V. 2015. The association between sterilizing activity and drug distribution into tuberculosis lesions. Nat Med 21:1223-7.
17. Jayaram R, Shandil RK, Gaonkar S, Kaur P, Suresh BL, Mahesh BN, Jayashree R, Nandi V, Bharath S, Kantharaj E, Balasubramanian V. 2004. Isoniazid pharmacokinetics-pharmacodynamics in an aerosol infection model of tuberculosis. Antimicrob Agents Chemother 48:2951-7.
18. Raghunandanan S, Jose L, Kumar RA. 2018. Dormant *Mycobacterium tuberculosis* converts isoniazid to the active drug in a Wayne's model of dormancy. J Antibiot (Tokyo) 71:939-949.
19. Gumbo T, Louie A, Liu W, Brown D, Ambrose PG, Bhavnani SM, Drusano GL. 2007. Isoniazid bactericidal activity and resistance emergence: integrating pharmacodynamics and pharmacogenomics to predict efficacy in different ethnic populations. Antimicrob Agents Chemother 51:2329-36.
20. Ahmad Z, Klinkenberg LG, Pinn ML, Fraig MM, Peloquin CA, Bishai WR, Nuermberger EL, Grosset JH, Karakousis PC. 2009. Biphasic kill curve of isoniazid reveals the presence of drug-tolerant, not drug-resistant, *Mycobacterium tuberculosis* in the guinea pig. J Infect Dis 200:1136-43.

Figure legends

Fig.1. AN12855 at 100 mg/kg is more effective and exhibits lower emergence of drug resistance than isoniazid at 25 mg/kg in C3HeB/FeJ mice with advanced lung pathology. Mice were infected by low dose aerosol with *Mycobacterium tuberculosis* Erdman 68 days prior to the start of treatment (week 0). Treatments were administered 5 of 7 days per week, Monday-Friday. AN12855 was formulated in 0.1% [v:v] tween-80, 1% [v:v] methyl cellulose 400 cP. Isoniazid was formulated in sterile water. Solid lines depict lung CFU burdens. Dashed lines depict drug-resistant escape mutants. Closed circles, untreated controls. Open triangles, isoniazid-treated. Closed triangles, AN12855-treated. The horizontal dotted line represents the lower limit of detection for drug-resistant isolate detection.

Fig. 2. Penetration and retention of isoniazid and the diazaborine AN12855 into different tissue compartments by pharmacokinetic analysis. (A) Gross pathology of a representative *Mycobacterium tuberculosis* Erdman infected C3HeB/FeJ lung lobe showing a Type I caseous lesion (square). (B) Micrograph of a Type I caseous lesion (hematoxylin and eosin stained). (C) Structures of AN12855 and isoniazid. (D) Quantitative drug distribution by tissue compartment over time. Mice were sampled after seven consecutive days of treatment with isoniazid at 25 mg/kg or AN12855 at 100 mg/kg. Time points were 0.5, 6 and 24 hours following administration for isoniazid (open triangles) and 2, 6 and 24 hours following administration of AN12855 (closed triangles). (E) Mean drug levels by compartment with each drug treatment. Inset, shows a magnification of the regions of interest. BLQ, below limits of quantification (< 1 ng/mL)

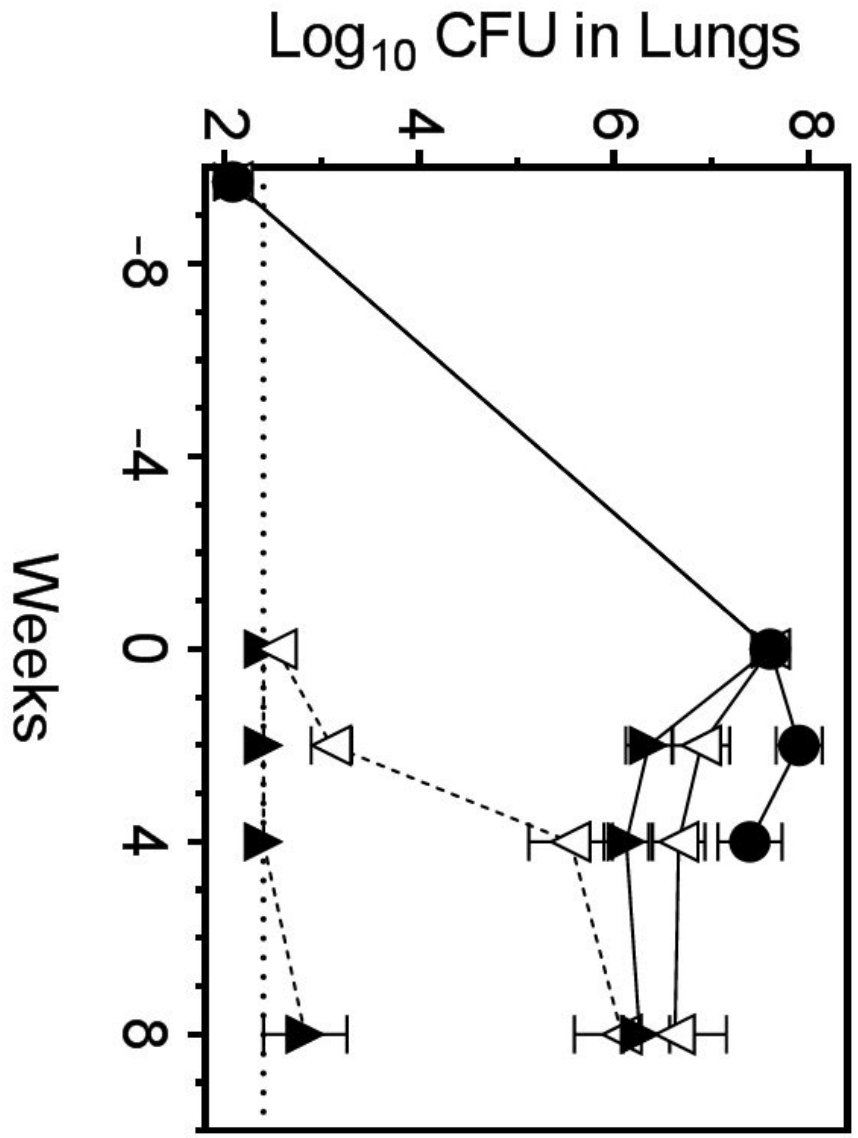

Table 1. Efficacy and drug resistance of AN12855 and isoniazid in the C3HeB/FeJ mouse model.

Group	Time point sampled			
	Start of treatment	2 week	4 week	8 week
Lung Efficacy (mean ± SEM, n)				
Vehicle Only	7.61 ± 0.18, 8/8	7.91 ± 0.24, 7/7	7.40 ± 0.33, 7/7	na
Isoniazid (25 mg/kg)	-	6.90 ± 0.29, 8/8	6.67 ± 0.27, 7/7	6.63 ± 0.53, 7/7
AN12855 (100 mg/kg)	-	6.36 ± 0.24, 8/8	6.13 ± 0.23, 8/8	6.27 ± 0.11, 8/8
Drug Resistance (mean ± SEM, (range), n, % resistance)				
Isoniazid	≤2.63 ± 0.09, (<2.40-3.00), 6/8, 0.001%	≤3.10 ± 0.21, (<2.40-3.89), 6/8, 0.016%	5.56 ± 0.43, (3.24-6.64), 7/7, 8%	6.09 ± 0.49, (3.77-7.71), 7/7, 29%
AN12855	<2.40 ± 0.00, (<2.40), 0/8, <0.0006%	<2.40 ± 0.00, (<2.40), 0/8, <0.011%	<2.40 ± 0.00, (<2.40), 0/8, <0.019%	≤2.83 ± 0.43, (<2.40-5.44), 1/8, 0.037%

Table 2. MICs of *M. tuberculosis inhA* promoter and coding sequence mutants

Strain	Source	SNPs		liquid MIC in μM (~fold shift versus Erdman)		
		fabG1-inhA promoter (nt)	InhA	Rifampicin	Isoniazid	AN12855
Erdman	Parent	na	na	0.01	0.44	0.16
ED-DPR18-RM4	*in vivo*	No SNP	G96V	0.007	0.83	> 20 (>122)
ED-DPR18-RM1	*in vitro*	No SNP	G96A	0.018	0.44	14.2 (87)
ED-DPR19-RM2	*in vitro*	C-15T	No SNP	0.02	3.2 (7)	1.1 (7)

Abbreviations: nt, nucleotide; na, not applicable; No SNP, no single nucleotide polymorphism

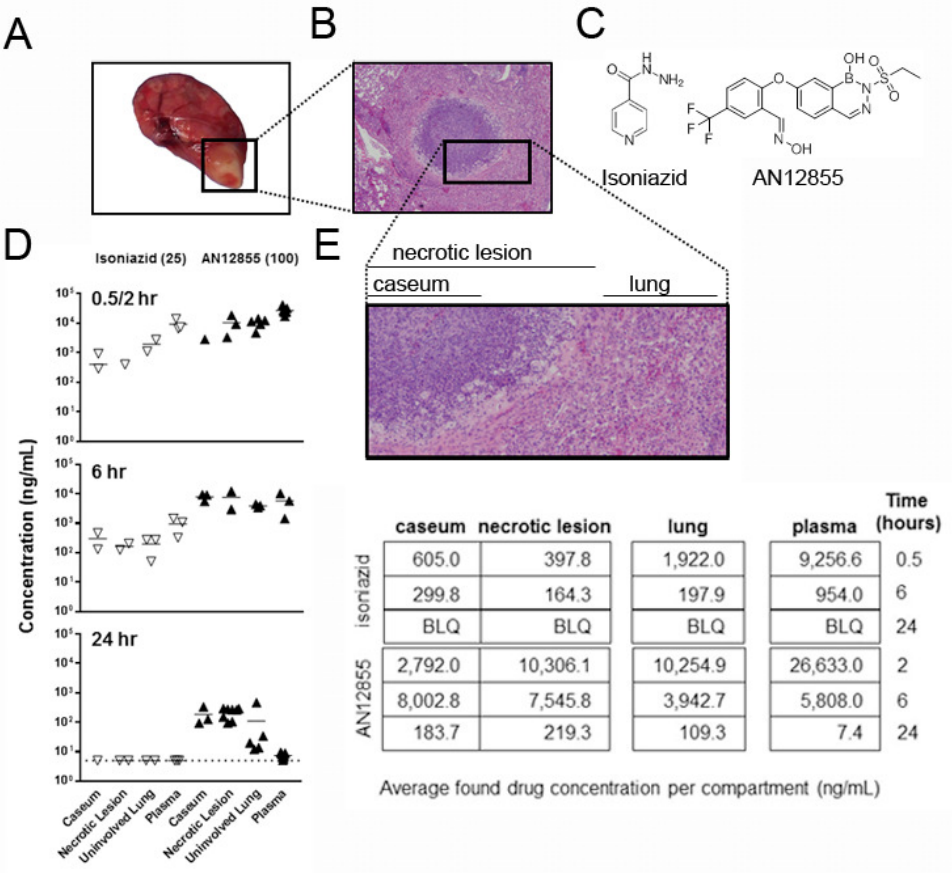

	caseum	necrotic lesion	lung	plasma	Time (hours)
isoniazid	605.0	397.8	1,922.0	9,256.6	0.5
	299.8	164.3	197.9	954.0	6
	BLQ	BLQ	BLQ	BLQ	24
AN12855	2,792.0	10,306.1	10,254.9	26,633.0	2
	8,002.8	7,545.8	3,942.7	5,808.0	6
	183.7	219.3	109.3	7.4	24

Average found drug concentration per compartment (ng/mL)